Optical Materials 96 (2019) 109298

Contents lists available at ScienceDirect

Optical Materials

journal homepage: www.elsevier.com/locate/optmat

SERS-active Ag–Al alloy nanoparticles with tunable surface plasmon resonance induced by laser ablation

Wenfeng Sun[a], Ruijin Hong[a,*], Qingyou Liu[b], Zhengwang Li[a], Jingqi Shi[a], Chunxian Tao[a], Dawei Zhang[a]

[a] Engineering Research Center of Optical Instrument and System, Ministry of Education and Shanghai Key Lab of Modern Optical System, University of Shanghai for Science and Technology, No.516 Jungong Road, Shanghai, 200093, China
[b] Key Laboratory of High-temperature and High-pressure Study of the Earth's Interior, Institute of Geochemistry, Chinese Academy of Sciences, Guiyang, 550081, China

ARTICLE INFO

Keywords:
Ag-Al alloy NPs
LSPR
SERS
FDTD

ABSTRACT

A series of Ag–Al alloy nanoparticles (NPs) were obtained on the silica substrates by ablating the Ag/Al bilayer thin film with an Nd:YAG fiber pulsed laser at ambient conditions. The corresponding tunability of localized surface plasmon resonance (LSPR) properties and the enhancement of Raman scattering intensity were realized due to the various Ag–Al alloy nanosphere sizes and states of aggregation by varying laser powers. With the increase of laser power, the crystalline quality of Ag–Al alloy NPs was improved with a red shift of the surface plasmon resonance wavelength from 432 nm to 484 nm. Furthermore, the simulation result of finite-difference time-domain (FDTD) showed a substantial agreement with experimental results.

1. Introduction

Due to the high detection sensitivity, there has been a focus on research in Surface-enhanced Raman spectroscopy (SERS) for many years since its discovery in 1970s [1–3]. SERS has been widely used as an important spectroscopic tool for biology, near field optics, nanoscience, medicine, and environmental monitoring [4–8]. Nowadays, there are two main mechanisms of electromagnetic (EM) enhancement and chemical enhancement to explain the SERS effect. In general, the EM enhancement plays a dominant role, and it mainly associated with large local fields caused by localized surface plasmon resonance (LSPR) [9]. In other words, an excellent SERS substrate would be obtained by preparing metal nanoparticles (NPs) which have good LSPR properties.

According to the previous research, coinage-metal such as gold, silver (Ag) and copper can provide a huge SERS effect when the metal nanostructures are in several tens of nanometers in size [10,11]. Ag is a very desirable material of SERS active substrate among these metals due to its strong and tunable surface plasmon resonance from the visible to near infrared spectral regions [12,13]. Nowadays, there are a great number of methods which contain wet chemical techniques, electron-beam lithography, focused-ion beam and photon lithography to fabricate metal nanostructures [14–16]. The advantages of these techniques are that they can fabricate SERS active nanostructures with a wide range of geometries, large-scale uniformity and good reproducibility [17]. Nevertheless, the methods above are facing problems with the intricate operation and significant cost due to the introduction of other reagents or the requirement of high vacuum environment. Thus, it is of great significance to develop a cost-effective and high-through-put method to fabricate SERS active nanostructures.

It is known that Ag follows the Volmer-Weber growth mode [18], in which the deposited Ag atoms initially form isolated islands. The pure Ag nanostructure is very difficult to be deposited on the substrate by laser ablation. Accordingly, through the incorporation of aluminum (Al) suppressing the 3D island growth of Ag and facilitating the formation of Ag–Al alloy NPs [19]. We herein propose a facile and cost-effective technique, pulsed laser ablation, to fabricate the Ag–Al alloy NPs. The surface plasmon resonance wavelength of the NPs can be tuned effectively by varying laser power. The influences of laser power on the structure, optical absorption and Raman scattering properties of NPs were also investigated. Moreover, the finite difference time domain (FDTD) method was employed to calculate electric field distribution of NPs.

2. Experiment

Prior to deposition, silica substrates were ultrasonically cleaned in acetone, ethanol and deionized water for 15 min respectively, and were subsequently dried with a flow of nitrogen. The deposition chamber

* Corresponding author.
E-mail address: rjhong@usst.edu.cn (R. Hong).

https://doi.org/10.1016/j.optmat.2019.109298
Received 3 May 2019; Received in revised form 30 July 2019; Accepted 5 August 2019

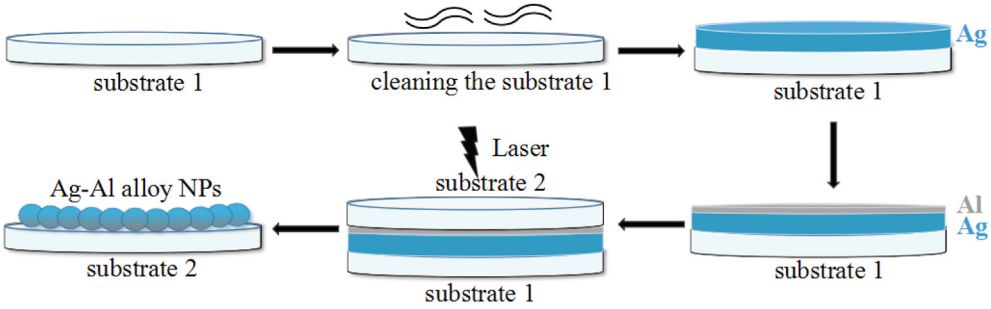

Fig. 1. A schematic diagram of the experiment process.

was evacuated to a base pressure of less than 5×10^{-4} Pa. Then, Ag thin film and Al thin film with the respective thickness of 10 nm and 1 nm were deposited on the silica substrates successively by electron beam evaporation at room temperature. The thickness of the film was monitored by a quartz crystal microbalance. Following the deposition, the blank silica substrates were covered on the surface of Ag/Al bilayer film and the laser ablation was processed by an Nd:YAG fiber pulsed laser with a wavelength of 1064 nm at ambient condition. The laser parameters were as follow: laser beam power were set as 0.5, 1, 1.5, 2, 2.5 and 3 W, respectively, the beam diameter was 0.01 mm, the pulse width was 100 ns, the frequency was 55 kHz, the scanning line spacing was 0.01 mm and the scan speed was set at 600 mm/s. For comparison, the single Ag thin film with thickness of 10 nm was also prepared in the study. The Ag–Al alloy NPs were marked as sample 1 (S1), sample 2 (S2), sample 3 (S3), sample 4 (S4), sample 5 (S5), sample 6 (S6), respectively, which are in accord with the increasing laser power (0.5–3 W). To better understand the process, a schematic of the experiment process is shown in Fig. 1.

The structural properties and the crystallinity of the samples were characterized by X-ray diffraction (XRD) using a Rigaku MiniFlex600 system with Cu kα radiation (λ = 0.15408 nm). The surface morphology were examined with atomic force microscopy (AFM)(XE-100, Park System) with the scanning area of 3 μm × 3 μm as well as scanning electron microscope (SEM) (S-4800, Hitachi). Thermo Scientific K-Alpha+ was used to study on the XPS. The optical absorption of the samples was measured with an UV–vis–NIR double beam spectrophotometer (Lambda 1050, Perkins Elmer). Raman scattering spectra were obtained by using a confocal microprobe Raman system (inVia Raman Microscope, Renishaw) with 633 nm laser. All the measurements were carried out at room temperature.

3. Results and discussion

3.1. Structural properties

Fig. 2 reveals the XRD patterns of Ag thin film and Ag–Al alloy NPs.

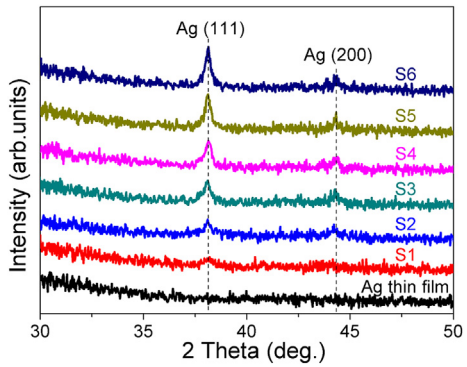

Fig. 2. XRD patterns of Ag thin film and Ag–Al alloy NPs.

The Ag film exhibit isolated island distribution when the thickness is very thin due to the Volmer-Weber growth mode of Ag [19]. Thus the Ag film with 10 nm thickness, too thin to vary the phase of the film from an amorphous state to a polycrystalline state, cannot be observed the diffraction peak. There are two diffraction peaks at around 38.2° and 44.5° in Ag–Al alloy NPs, which corresponds to the (111) and (200) crystal plane of Ag (JCPDS: 04–0783). As shown in Fig. 2, the highly intense diffraction peak was located at 38.2°, indicating a preferential orientation of the silver grains along the (111) crystallographic direction [20]. Typically, for non-epitaxial deposition on a substrate, the film structure tends to be a (111) or (001) plane because these planes exhibit minimal surface free energy [21]. It means that the (111) textured film must form an effective equilibrium state in which sufficient surface mobility is imparted under certain deposition conditions to strike the atoms. With stronger laser power, the diffraction peak intensity of Ag–Al alloy NPs tends to gradually increase, which can be attributed to the recrystallization of crystal grain. The study shows that laser ablation has a significant influence on the grain growth of Ag–Al NPs film.

3.2. Surface morphology

Fig. 3(a) and (b) shows the representative AFM micrographs with a scanning area of 3 μm × 3 μm obtained from Ag thin film and Ag–Al alloy NPs with laser power of 3 W. The morphology of Ag thin film exhibits consecutive and smooth with the values of the root mean square (RMS) surface roughness of Ag thin film is 2.532 nm. After laser ablation, the alloy particles deposited on another substrate and exhibited spherical or ellipsoidal structures. It means that good textured Ag–Al alloy NPs can be obtained by laser ablation. Fig. 3(c) and (d) show the SEM images of Ag thin film and Ag–Al alloy NPs with laser power of 3 W. Ag thin film consisted of fine island-like grains with sizes ranging from 10 to 20 nm, while Ag–Al alloy NPs film made up of ellipsoidal structures with size about 80–150 nm. It is apparent that laser irradiation breaks Ag thin film into defined particles which have a discontinuous structure. These SEM results are consistent with those of in AFM images.

The RMS surface roughness Ag–Al alloy NPs are 9.724, 10.176, 10.951, 11.295, 11.981 and 12.366 nm, respectively, as shown in Fig. 4(a). The laser-induced thermo-elastic force causes the alloy particles to peel off from the bilayer sample [22]. Thereby, the as-deposited film with consecutive surface was transformed into orderly spheroidal structure. When the laser power is 0.5 W, the amount of alloy particles peeled off is relatively small due to the low laser energy, resulting in the limited collections between alloy particles and then forming clusters with small size [23]. As shown in Fig. 4(b), with the increase of laser power, the average particle size of Ag–Al alloy NPs also increases, which is consistent with the RMS surface roughness results.

3.3. Composition and valence state

Fig. 5 shows the XPS spectra of Ag–Al alloy NPs with laser power of 3 W. As shown in Fig. 5(a), the Al, C, Ag, Na and O peaks can be

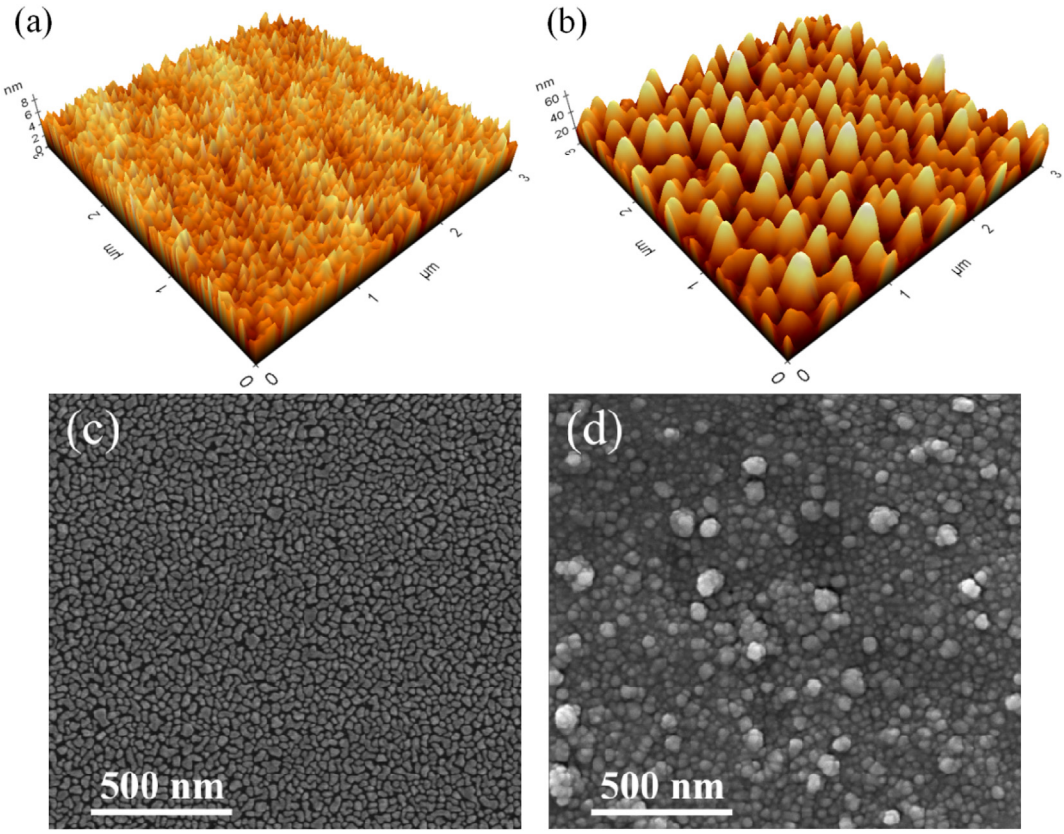

Fig. 3. AFM images of (a) Ag thin film and (b) Ag–Al alloy NPs with laser power of 3 W. SEM images of (c) Ag thin film and (d) Ag–Al alloy NPs with laser power of 3 W.

observed. The peak of O1s may be derived from the oxide of Al. Peaks such as NaKL1 and Na1s are from the silica substrate. There is no potential contamination during the laser ablation process, and has no impact on subsequent research. According to Fig. 5(b), two peaks at approx. 368.3 eV and 374.3 eV are observed in samples, belonging to $3d_{5/2}$ and $3d_{3/2}$ of Ag atom [24,25], respectively. The Ag $3d_{5/2}$ peak appearing at 367.2–367.7 eV corresponds to oxidized states such as Ag_2O and AgO [26–28]. However, no peak in the XPS spectra appears in this binding energy range, indicating that no appreciable oxidation occurred during laser irradiation. In Fig. 5(c), an independent peak at around 73.2 eV corresponds to 2p of Al atom can be detected. The binding energy of Al_2O_3 (i.e., 74.9 eV) is higher than 73.2 eV, while the metallic Al (i.e., 72.6 eV) is lower than 73.2 eV [29,30]. That is, most of Al in the alloy NPs was activated to form Al–O-related chemical bonds. As shown in Table 1, the relative content of Ag in Ag–Al alloy NPs can be obtained by analyzing the XPS peak areas of Ag $3d_{5/2}$ peak and Al 2p peak. As the laser power increases, the Ag content gradually increases from 54.48% to 91.56%, while the Al content decreases accordingly. As a result, the oxidation of Al and the decrease of Al content induced the variation of local dielectric environment in Ag–Al alloy NPs. Combined with the optical absorption discussed in section 3.4, our experimental results demonstrate that Al plays an important role in tuning the LSPR wavelength.

3.4. Optical absorption

The plasmon resonance peaks observed in the absorption spectrum can well reflect the variety of local electromagnetic field between the NPs, which plays an important role in the enhancement of SERS. Fig. 6 shows the absorption spectra of Ag 10 and Ag–Al alloy NPs. According to Fig. 6(a), the Ag 10 exhibits strong absorption in the visible range with broad absorption band because of the continuous film structure.

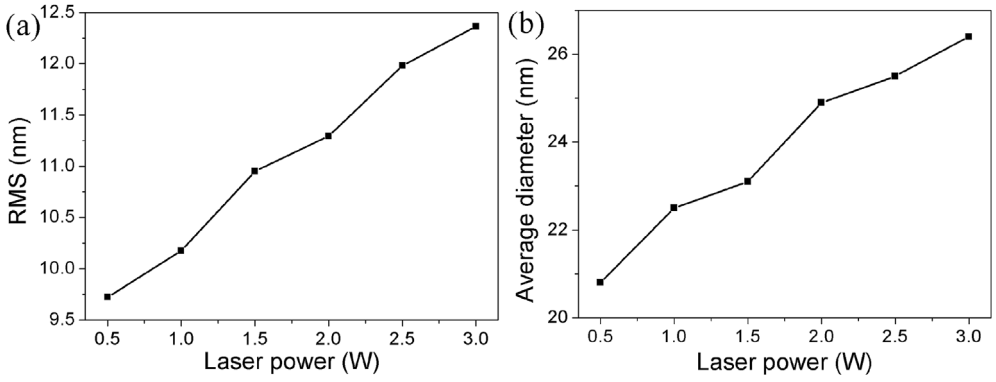

Fig. 4. (a) The surface roughness of Ag–Al alloy NPs corresponding to various laser power. (b) The average diameter of Ag–Al alloy NPs with different laser power.

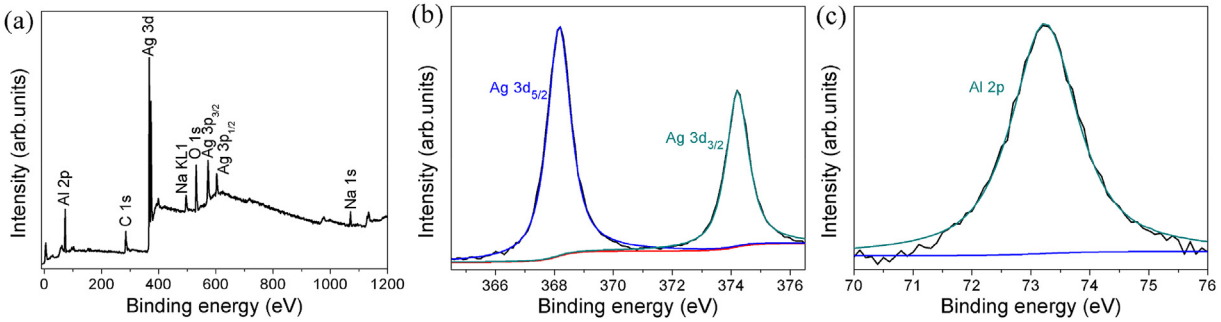

Fig. 5. XPS spectra of Ag–Al alloy NPs with laser power of 3 W: (a) survey spectrum, (b) Ag 3d and (c) Al 2p.

Table 1
Composition ratios of Ag–Al alloy of as-ablated samples.

Sample	S1	S2	S3	S4	S5	S6
Ag	54.48%	63.33%	68.24%	75.36%	82.64%	91.56%
Al	45.52%	36.67%	31.76%	24.64%	17.36%	8.44%

However, the absorption peaks of Ag–Al alloy NPs shift to the shorter wavelength with a relatively narrowed peak after laser ablation. For Ag–Al alloy NPs with increasing gradually laser power from 0.5 to 3 W, the LSPR wavelength shows a red shift from 432 nm to 484 nm. At the same time, the LSPR peaks were also enhanced in intensity. In Fig. 6(b), there is a wave crest which represents the wavelength corresponding to the maximum absorption in each absorption spectrum, and the value of these wavelengths is 432, 438, 454, 464, 474 and 484 nm, respectively.

According to Fig. 6, the LSPR peak of the alloy NPs can be tuned effectively by varying the power of the laser irradiation. As is known, structured thin films will be more prone to LSPR [31]. Therefore, no LSPR absorption peak of Ag thin film can be observed due to its non-structured and consecutive surface [32]. However, when the pulsed laser is applied to ablate the Ag/Al bilayer film, a great quantity of metallic particles was peeled and formed the nanosphere structures which enable LSPR peak in samples. According to the Gans theory, a classical quasistatic theory for calculating the light absorption of NPs in ellipsoidal structures, the plasmon wavelength and absorption cross-section vary with the particles size and shape [33].

Greater laser power will cause larger size of the NPs which has higher absorption cross-sections, leading to the enhancement of LSPR peak intensity. Meanwhile, the introduction of Al can cause the changes of local dielectric environment between particles. When the incident light is absorbed by the Ag–Al alloy NPs, the local electromagnetic field coupling will take place between the particles, which acts as a critical role in regulating the peak position of the LSPR. As the laser power increases, the content of the Al in the Ag–Al alloy NPs will decrease, the size of the Ag–Al alloy NPs will increase in the meantime. As a result, the LSPR resonance peak appears a red shift, which is well predicted by the Maxwell–Garnett (MG) theory [34].

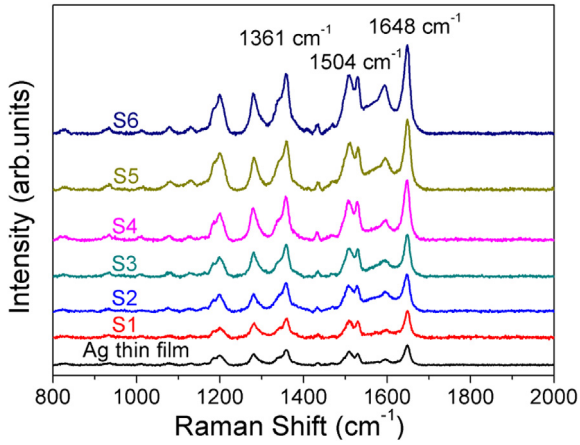

Fig. 7. Raman scattering spectra of Rh B on Ag thin film and Ag–Al alloy NPs with different laser power.

3.5. SERS performance

In order to prove the superiority of the SERS performance of Ag–Al alloy NPs, both Ag thin film and Ag–Al alloy NPs were used as SERS substrates. The probing molecule Rhodamine B (Rh B) is a typical artificial dye and was chosen as a test compound for researching the application of the samples. In this study, the Rh B molecule solutions with the concentration of 10^{-4} mol/L are drop deposited onto the surface of samples. As shown in Fig. 7, Ag thin film and Ag–Al alloy NPs

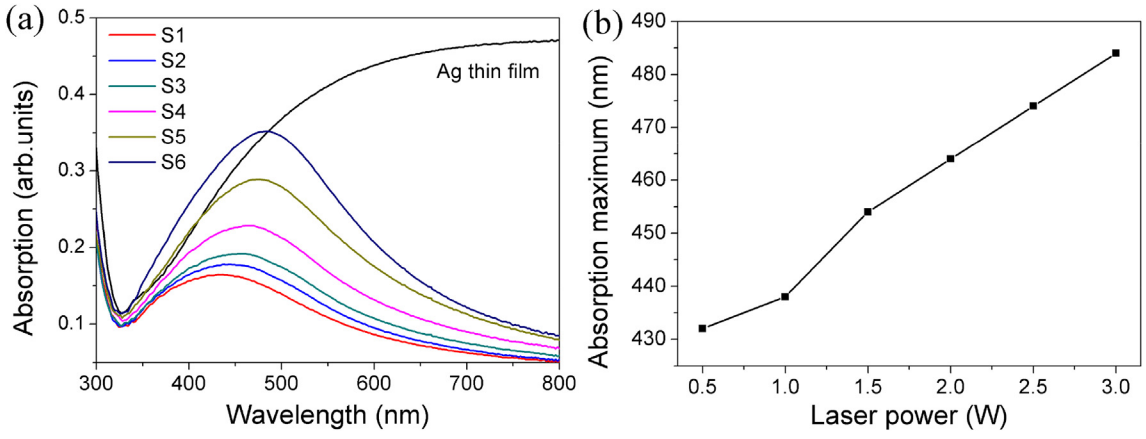

Fig. 6. (a) Absorption spectra of Ag thin film and Ag–Al alloy NPs with various laser power; (b) Absorption maximum.

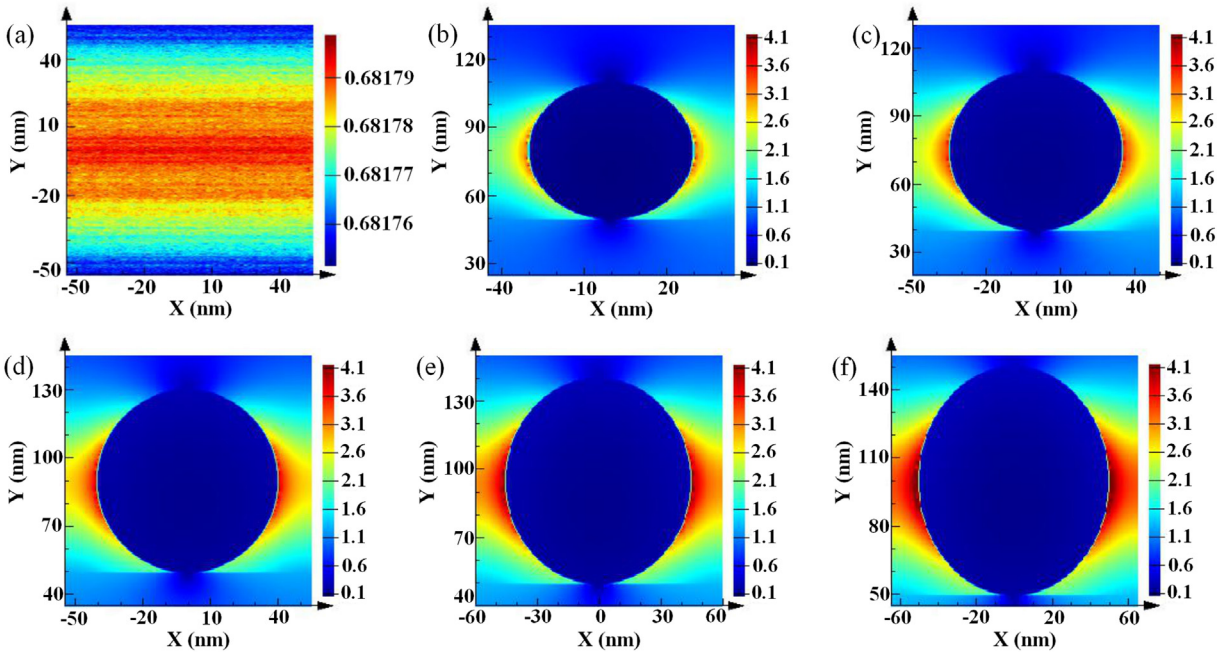

Fig. 8. FDTD simulated electric field amplitude patterns for (a) Ag thin film and (b)–(f) Ag–Al alloy NPs with various particle sizes and different content of Ag.

can be measured the Raman peaks of Rh B. Due to the aromatic stretch vibrations of the chromophore [35], three strongest Raman peaks can be found at about 1648, 1361 and 1504 cm^{-1}, which being assigned to C = C stretching modes of aromatic rings. After laser ablation, the SERS signal intensity of the Ag–Al alloy NPs have been significantly enhanced compared to Ag thin film. In the meantime, the Raman signal intensities show an increasing trend with laser power between 0.5 W and 3 W. Apparently, the SERS enhancement of alloy NPs samples can be flexibly adjusted by varying laser power.

The excitation of surface plasmon resonance can result in a shift in the optical resonance properties of coinage-metal nanostructures, causing the local electromagnetic field enhanced significantly, thereby generating the enhancement of SERS [12,36]. According to the absorption spectrum discussed in section 3.4, the Ag–Al alloy NPs have a good LSPR performance than Ag thin film, resulting in a better SERS performance. In accordance with the electromagnetic enhancement theory [37], the Ag thin film has non-structured and smooth surface which causes the less tips or "hot spots", resulting in weakening of both the local electrical fields and SERS enhancement. Conversely, the alloy NPs irradiated by the laser possess more tips and "hot spots", which generate stronger local electromagnetic field. As the laser power increases, the size of Ag–Al alloy NPs become larger which generating higher Raman cross-section, leading to a gradual increase in the intensity of the Raman signal. In consequence, the alloy NPs samples exhibit structured and rougher surface leading to the SERS enhancement [38], as shown in Fig. 7. The SERS enhancement is also correspond with the variation trend of the surface roughness simultaneously in Fig. 4(a).

To further verify the conclusions above, the simulation of FDTD was used to calculate the electric field distribution for all samples. In this simulation, a 633 nm laser irradiated perpendicularly to the x-y plane of the samples with the polarization along the y-axis direction. Fig. 8 illustrates the electric field intensity of Ag thin film and Ag–Al alloy NPs. The electric field intensity of the Ag thin film is weak due to the smooth surface, while the electric field strength of Ag–Al alloy NPs is stronger, which shows the consistency of the above SERS performance. Fig. 8(b)–(f) exhibit the spatial distribution of the electric field intensity of Ag–Al alloy NPs with various particle sizes and different content of Ag, respectively. The tip or "hot spot" formed on the localized surface between the spacing of NPs, and the intensity of the electric field increases significantly as the lager NPs and the content of Ag increases. On the whole, the increase in particle size and the content of Ag lead to a gradual increase of SERS intensity, which can be attributed to the stronger intensity of tips or "hot spots". The simulation results are well consistent with the experimental results above.

4. Conclusions

In conclusion, the SERS performance of Ag–Al alloy NPs which were tuned by laser ablation with different laser power has been studied in this paper. The results show that the LSPR wavelength of Ag–Al alloy NPs shows an obvious red shift by varying the laser power. Moreover, the Raman scattering intensities were observed to be obviously enhanced because of the lager particle size and the states of aggregation of Ag–Al alloy NPs, which is consistent with the results of FDTD simulation. These findings provide a cost-effective and simple way to fabricate SERS active substrate, which might play a crucial part in the development of practical applications of nanoscience.

Declaration of interest statement

We declare that we have no financial and personal relationships with other people or organizations that can inappropriately influence our work, there is no professional or other personal interest of any nature or kind in any product, service and/or company that could be construed as influencing the position presented in, or the review of, the manuscript entitled.

Acknowledgments

This work was partially supported by the National Natural Science Foundation of China (61775140, 61775141), and the Shanghai foundation for Science and technology innovation action plan (15441902302, 1714220060).

References

[1] M. Fleischmann, P.J. Hendra, A.J. McQuillan, Raman spectra of pyridine adsorbed at a silver electrode, Chem. Phys. Lett. 26 (1974) 163–166.

[2] D.L. Jeanmaire, R.P. Van Duyne, Surface Raman spectroelectrochemistry. Part I. Heterocyclic, aromatic, and aliphatic amines adsorbed on the anodized silver electrode, J. Electroanal. Chem. 84 (1977) 1–20.
[3] M.G. Albrecht, J.A. Creighton, Anomalously intense Raman spectra of pyridine at a silver electrode, J. Am. Chem. Soc. 99 (1977) 5215–5217.
[4] O. Guselnikova, P. Postnikovb, A. Pershina, V. Svorcika, O. Lyutakov, Express and portable label-free DNA detection and recognition with SERS platform based on functional Au grating, Appl. Surf. Sci. 470 (2019) 219–227.
[5] Y. Kalachyova, O. Guselnikova, R. Elashnikov, I. Panov, J. Žádný, V. Církva, J. Storch, J. Sykora, K. Zaruba, V. Švorčík, O. Lyutakov, Helicene-SPP-Based chiral plasmonic hybrid structure: toward direct enantiomers SERS discrimination, ACS Appl. Mater. Interfaces 11 (2019) 1555–1562.
[6] S. Lee, M.G. Hahm, R. Vajtai, D.P. Hashim, T. Thurakitseree, A.C. Chipara, P.M. Ajayan, J.H. Hafner, Utilizing 3D SERS active volumes in aligned carbon nanotube scaffold substrates, Adv. Mater. 24 (2012) 5261–5266.
[7] S. Nie, S.R. Emory, Probing single molecules and single nanoparticles by surface-enhanced Raman scattering, Science 275 (1997) 1102–1106.
[8] M. de Veij, P. Vandenabeele, T. De Beer, J.P. Remon, L. Moens, Reference database of Raman spectra of pharmaceutical excipients, J. Raman Spectrosc. 40 (2009) 297–307.
[9] M. Moskovits, Surface roughness and the enhanced intensity of Raman scattering by molecules adsorbed on metals, J. Chem. Phys. 69 (1978) 4159–4161.
[10] M. Moskovits, Surface-enhanced spectroscopy, Rev. Mod. Phys. 57 (1985) 783–826.
[11] J.F. Li, R. Panneerselvam, Z.Q. Tian, Shell-Isolated nanoparticle-enhanced Raman spectroscopy, Nature (2010) 08907392-395.
[12] S.Y. Ding, J. Yi, J.F. Li, B. Ren, D.Y. Wu, R. Panneerselvam, Z.Q. Tian, Nanostructure-based plasmon-enhanced Raman spectroscopy for surface analysis of materials, Nat. Rev. Mater. 16036 (2016) 1–16.
[13] Y.F. Chan, C.X. Zhang, Z.L. Wu, D.M. Zhao, W. Wang, H.J. Xu, X.M. Sun, Ag dendritic nanostructures as ultrastable substrates for surface-enhanced Raman scattering, Appl. Phys. Lett. 102 (2013) 183118.
[14] A. Gopinath, S.V. Boriskina, W.R. Premasiri, L. Ziegler, B.M. Reinhard, L. Dal Negro, Plasmonic nanogalaxies: multiscale aperiodic arrays for surface-enhanced Raman sensing, Nano Lett. 9 (2009) 3922–3929.
[15] M.J. Banholzer, J.E. Millstone, L. Qin, C.A. Mirkin, Rationally designed nanostructures for surface-enhanced Raman spectroscopy, Chem. Soc. Rev. 37 (2008) 885–897.
[16] R.J.C. Brown, M.J.T. Milton, Nanostructures and nanostructured substrates for surface-enhanced Raman scattering (SERS), J. Raman Spectrosc. 39 (2008) 1313–1326.
[17] A. Shiohara, Y. Wang, L.M. Liz-Marzán, Recent approaches toward creation of hot spots for SERS detection, J. Photochem. Photobiol., A C 21 (2014) 2–25.
[18] R.S. Sennett, G.D. Scott, The structure of evaporated metal films and their optical properties, J. Opt. Soc. Am. 40 (1950) 203.
[19] C. Zhang, D. Zhao, D. Gu, H. Kim, T. Ling, Y.K.R. Wu, L.J. Guo, An ultrathin, smooth, and low-loss Al-doped Ag film and its application as a transparent electrode in organic photovoltaics, Adv. Mater. 26 (2014) 5696–5701.
[20] R.J. Hong, X.H. Wang, J.L. Ji, C.X. Tao, D.W. Zhang, ITO induced tunability of surface plasmon resonance of silver thin film, Appl. Surf. Sci. 356 (2015) 701–706.
[21] P.B. Petrov, L. Barna, J. Hultman, E. Greene, Microstructural evolution during film growth, J. Vac. Sci. Technol. A 21 (2003) 117–128.
[22] Y. Oh, M. Lee, Single-pulse transformation of Ag thin film into nanoparticles via laser-induced dewetting, Appl. Surf. Sci. 399 (2017) 555–564.
[23] P.K. Diwakar, S.S. Harilal, N.L. LaHayea, A. Hassaneina, P. Kulkarni, The influence of laser pulse duration and energy on ICP-MS signal intensity, elemental fractionation, and particle size distribution in NIR fs-LA-ICP-MS, J. Anal. At.Spectrom. 28 (2013) 1420–1429.
[24] T. Kaspar, T. Droubay, S. Chambers, P. Bagus, Spectroscopic evidence for Ag(III) in highly oxidized silver films by X-ray photoelectron spectroscopy, J. Phys. Chem. C 114 (2010) 21562.
[25] A. Ferraria, A. Carapeto, A. Rego, X-ray photoelectron spectroscopy: silver slats revisited, Vacuum 86 (2012) 1998.
[26] Y. Oh, M. Lee, Single-pulse transformation of Ag thin film into nanoparticles via laser-induced dewetting, Appl. Surf. Sci. 399 (2017) 555–564.
[27] G. Hoflund, J. Weaver, W. Epling, Ag2O XPS spectra, Surf. Sci. Spectra 3 (1994) 157.
[28] G. Hoflund, J. Weaver, W. Epling, AgO XPS spectra, Surf. Sci. Spectra 3 (1994) 163.
[29] J.F. Silvain, J.C. Bihr, M. Alnot, J. Lambert, J.J. Ehrhardt, X-ray photoelectron spectroscopy and transmission electron microscopy studies of the NiAl/Al2O3 interfacial chemical compatibility, J. Vac. Sci. Technol. A 13 (1995) 1893.
[30] F. Meng, F. Ge, Y. Chen, G. Xu, F. Huang, Local structural changes induced by ion bombardment in magnetron sputtered ZnO: Al films: Raman, XPS, and XAS study, Surf. Coat. Technol. 365 (2019) 2–9.
[31] S.A. Maier, Plasmonics: Fundamentals and Applications vol. 52, Springer, 2007, pp. 49–74.
[32] W. Wei, R. Hong, Y. Meng, C. Tao, D. Zhang, Electron-beam irradiation induced phase transformation, optical absorption and surface-enhanced Raman scattering of Indium tin alloy thin films,Superlattice, Microst 106 (2017) 189–196.
[33] H. Chen, L. Shao, Q. Li, J. Wang, Gold nanorods and their plasmonic properties, Chem. Soc. Rev. 42 (2013) 2679–2724.
[34] G. Xu, M. Tazawa, P. Jin, S. Nakao, Surface plasmon resonance of sputtered Ag films: substrate and mass thickness dependence, Appl. Phys. A 80 (2005) 1535–1540.
[35] T. Vosgröne, A.J. Meixner, Surface and resonance enhanced micro-Raman spectroscopy of xanthene dyes at the single-molecule level, J. Lumin. 107 (2004) 13–20.
[36] J.A. Creighton, C.G. Blatchford, M.G. Albrecht, Plasma resonance enhancement of Raman scattering by pyridine adsorbed on silver or gold sol particles of size comparable to the excitation wavelength, J. Chem. Soc., Faraday Trans. 2 (75) (1979) 790–798.
[37] M. Fan, A.G. Brolo, Silver nanoparticles self-assembly as SERS substrates with near single molecule detection limit, Phys. Chem. Chem. Phys. 11 (2009) 7381–7389.
[38] H.A. Chen, J.L. Long, Y.H. Lin, C.J. Weng, H.N. Lin, Plasmonic properties of a nanoporous gold film investigated by far-field and near-field optical techniques, J. Appl. Phys. 110 (2011) 054302.